J. Fluid Mech. (1967), *vol.* 29, *part* 2, *pp.* 259–272
Printed in Great Britain

Visualization of an incompressible wake with base bleed

By C. J. WOOD
Department of Engineering Science, University of Oxford

(Received 23 September 1966)

The wake behind a two-dimensional bluff body has been photographed in water in order to investigate the modifying effect of base bleed. With this technique it has been possible to measure velocities at chosen points and from these make simultaneous estimates of the base pressure and of the strength of individual vortices in the wake. The results suggest that the observed decay in the vortex structure of the wake is related to variations in the conditions of mixing between the base fluid and the external stream.

1. Introduction

It is well known that the drag of a two-dimensional body with a blunt trailing edge can be reduced by the ejection of a relatively small flow of fluid from the blunt edge. This device, commonly known as base bleed, has been studied both at supersonic and subsonic speeds (Nash 1962). It is interesting because of its potential value in several fields of fluid dynamics. In aircraft design, for instance, there is the possibility of maintaining the low drag characteristics of aerofoils, while eliminating the weight, the skin friction and also the supersonic wave drag of a long, tapering rear section. This is advantageous when there is available a supply of air, drawn perhaps from suction boundary layer control devices, which would otherwise be useless. Alternatively, in gas turbine practice, air may be required internally to cool turbine blades. Clearly, base bleed offers the hope of using that air to advantage afterwards.

Both these applications are associated with the disposal of waste fluid. They are emphasized here because if a sink drag is incurred, purely in order to collect the bleed fluid from the oncoming stream, then the overall drag reduction due to base bleed may well be too small to be of any practical importance.

From a more fundamental point of view, the relationship between drag and wake structure is a very important topic. Thus any device which offers a new way of studying that relationship is of great value. Base bleed is just such a device. Several wind-tunnel investigations have been carried out with the object of explaining the mechanism by which base bleed changes the drag and some illuminating results have been obtained. However, a limiting factor has always been that, while pressures can be measured very easily in a wind tunnel, the detailed examination of the wake vortex structure is more difficult.

In order to overcome this difficulty, it was decided to abandon conventional

wind-tunnel methods and rely instead on the increasingly popular technique of quantitative flow visualization. This method involves the direct measurement of local velocities from photographs of particles moving with the flow. Low velocity water flows provide the most convenient medium for this type of work. Also, by fixing the camera with respect to the undisturbed flow, a periodic wake flow is made to appear as an array of individual vortices having only a small induced velocity relative to the camera. These two facts dictated the choice of a static water tank facility with a moving model and a stationary camera.

With this apparatus, it was hoped that the actual strengths of individual wake vortices could be estimated, and also the base pressure, both from measurements of the approximate local velocities. The possibility of making these two measurements simultaneously offered the hope that a more positive conclusion might be reached concerning the relationship between the base drag and the changing strength of the vortex street. It is the attempt to do this that is described in the present report.

2. Apparatus

2.1. *The hydrostatic channel*

Flow visualization in static water channels is an old technique which is once again gaining popularity because of its extreme simplicity. Typical modern methods have been described recently by Clutter, Smith & Brazier (1962).

The present channel is 15 ft. long and 2 ft. wide with a depth of water up to 18 in. The sides and base are constructed of toughened plate glass. Horizontal rails are provided to carry a simple trolley supported on three ball-bearing rollers. Further rollers, running on the sides of one of the rails, provide the necessary lateral location.

To tow the trolley, a thin steel cable is passed in a helical groove twice round a pulley drum at one end of the channel and round an idler pulley at the far end. Both ends of the cord are secured to the trolley with sufficient tension to prevent slip at the drum. The latter is driven through a simple gearbox by a 25 W single-phase capacitor induction motor with a worm reduction gear. The worm gear reduces the synchronous speed of the output shaft to 52 rev/min with only 3 % reduction on full load. Alternative pairs of spur gears may be fitted rapidly to the gearbox to give nominal trolley speeds of 3·66, 5·21, 10·23 or 14·62 in./s.

Initial speed calibration tests were carried out with an $X-Y$ recorder, using a potentiomenter wire as a position transducer. These showed that the initial acceleration distance was not more than 2 or 3 ft. and that the speed thereafter was constant within $\pm 1\,\%$. However, the value of the final steady speed was found to depend slightly upon the static cable tension, so that periodic checks with a stopwatch were necessary.

For the present experiments, the lowest speed was used. The Reynolds number was then $2{\cdot}5 \times 10^4$ per foot and an aerofoil model of 6 in. chord could be expected to have laminar boundary layers. What was more important was that at this speed the question of Froude number effects did not arise, since the surface disturbances were barely visible.

For the base bleed flow a water supply to the trolley was required. This was

provided by drawing water from one end of the tank and pumping it past an orifice flow meter up to a swinging boom, which overhung the channel. From this the water was delivered through a flexible pipe to the top of the trolley.

2.2 *Illumination*

To visualize two-dimensional flows, the channel was designed for use with a model projecting vertically downwards from the trolley and ending just clear of the channel floor. A section of the flow was illuminated by a horizontal plane of light midway between the water surface and the floor.

To provide this illumination, four 1000 W mercury vapour lamps (Philips SP 900 W) were mounted horizontally in two aluminium cases. Each lamp was cooled by jets of compressed air. A biconvex lens in front of each lamp focused the light parallel to the horizontal plane and stray divergent light was removed by two horizontal collimating slits. Thus each box produced a 1 to 2 ft. wide divergent beam, whose uniform thickness could be varied up to 1 in. By replacing the two boxes facing each other on opposite sides of the channel, the illumination was made more uniform and shadows were eliminated.

The flow was made visible by a suspension of small (0·2 mm) polystyrene beads, introduced at the position of the light beam. The particles, already wetted in dilute detergent, were scattered evenly over the surface from a bottle with a fine sprinkler. This caused negligible disturbance to the water and the particles, having a specific gravity of about 1·05, sank slowly in a uniform cloud. As a portion of the cloud became illuminated, the moving model was made to pass through. A cam on the trolley then depressed a mechanical trigger to operate the camera shutter.

2.3. *Photography*

The scale and position of the photographs was established by photographing a grid of 2 in. squares inscribed on a perspex plate. This was mounted temporarily in the plane of the light beam and positioned accurately. The grid then served as an aid to accurate positioning and focusing of the camera, while a thin rod, suspended freely from the centre point of the grid, enabled the vertical alignment to be checked.

Photographs could be taken of the flow at any position relative to the model simply by moving the camera trigger along the side of the tank. Some specimen photographs from the present series of tests are shown in figures 2 to 7. They were taken with a half plate camera, using a lens of 208 mm focal length. To give particle streaks of a convenient length, the shutter time was set at approximately 0·13 s. The effective film exposure, or the quantity of light falling on a given point within a streak depends of course, not on the shutter time but varies inversely with the speed of the particle. It was found to be adequate at *f*. 11 with a film speed of A.S.A. 1200 (Kodak Royal X Pan). A slower film could have been used with a lens of wider aperture.

2.4. *Measurements of velocity*

For any particle moving with the fluid, the velocity may be determined from the length of the particle streak, the scale of the photograph and the time. With a

cheap shutter mechanism, the opening time is usually an inaccurate and variable quantity. However, the 100 c/s flashing of the mercury vapour lamps used in the present tests provided a simple alternative method of timing. On each photograph, particle streaks in the higher velocity regions appeared as rows of dots. A visibility time, usually slightly shorter than the actual shutter time, was therefore defined as $(n-1)/100$ s, where n was the number of dots in a streak. This time was the same for all particle streaks in a given photograph.

The streak lengths were measured with a travelling microscope, from the beginning of the first dot to the beginning of the nth dot. For short streaks, where the dots overlapped, each dot was assumed to be circular and the length was measured from one end of the streak up to the inner edge of an imaginary inscribed circle at the other. Clearly, in these measurements of short streaks there is the possibility of an estimating error. It could have been as much as $\pm 0{\cdot}2$ particle diameters; depending upon the quality of the photograph. This error reaches serious proportions in the very short streak lengths and sets a lower limit on the velocities, which can be measured with acceptable accuracy. A further error corresponding to $\pm 0{\cdot}005$ s (4 % on a 13-dot streak) occurred on some photographs because the camera shutter opened or closed during a flash and produced an incomplete dot. This error again applied to the short overlapping streaks only because on the long streaks it was possible to disregard the partial dot both in the length measurement and in the time count.

3. The model

For the present base bleed experiments, a simple two-dimensional aerofoil model was built of sheet brass. The section had an elliptic nose and a parallel rear section, which terminated in an open trailing edge (figure 1). The chord c was 6 in., and the base height h was 1·68 in. Because the walls were thin and the cavity

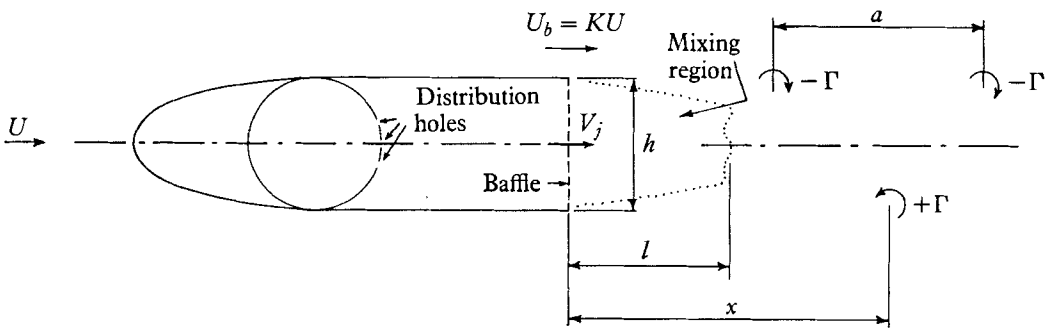

FIGURE 1. Diagram of model showing notation. $C_\mu = V_j/U$.

occupied virtually the whole thickness of the aerofoil, the bleed coefficient C_μ could be defined simply by the velocity ratio V_j/U of the jet to the free stream. The main spar of the model was a brass tube of 1·5 in. bore. This also served as a manifold to distribute the internal water supply. To provide uniform discharge along the span, an array of holes was drilled according to the one-dimensional manifold theory of Horlock (1956).

Calibration of the manifold by collecting the discharge in a partitioned tank showed that the discharge from the pipe was uniform within $\pm 5\,\%$. However, the development of a good uniform flow within the rear cavity of the model was hampered by the unfortunate tendency for the water jets to unite in groups or to adhere to the cavity walls. Also, the spanwise velocity component of the jets, which was not completely eliminated by the short distribution holes, caused a decrease in bleed velocity towards the supply end of the span.

The effect of both these faults was observed by stretching a stainless steel wire along the span just behind the immersed model and watching the motion of rows of hydrogen bubbles, generated electrolytically at the wire. It was seen that the velocity varied by 10–15 % along the whole span, while superimposed upon this variation were two short troughs of very low velocity near the ends. Fortunately the middle 50 % of the span showed very little variation.

Various combinations of perforated sheet brass baffles were used in an attempt to smooth the flow. However, these rapidly became blocked by bubbles and the final design employed only one baffle, positioned where it could be scrubbed vigorously before each run.

Fortunately, the importance of spanwise uniformity in the bleed flow itself is not great. Bearman (1966) has demonstrated that even when his bleed aperture was entirely blocked over part of the span, the effect on the base pressure was negligible.

Three-dimensional effects from the ends of the span also appeared to have no serious effect on the two-dimensional nature of the vortex street. Because the speed was low, the water surface remained effectively flat. At the other end, the 0·05–0·1 in. clearance between the model and the tank floor was insignificant. The circular motion of surface particles and of those on the bottom showed that each vortex line did extend over the whole span and terminated at these boundaries. The end effects normally associated with wind tunnel wall boundary layers do not, of course, exist in a static fluid.

4. The vortex formation process

Certain prominent features of base bleed flow are now well established. It is known that, while there is little change in the characteristic dimensions and frequency of the vortex street, base bleed causes the vortices to form progressively further from the body (Wood 1964; Bearman 1966). Bearman has also shown that the distance to vortex formation is a function of the base pressure.

A similar displacement of the vortex formation region appears in the present photographs (figures 2–7, plates 1–3) although the actual distance is difficult to define. In this case, a more clearly defined distance is an entrainment length, measured from the base to the downstream limit of the unmixed base fluid in the wake. This base fluid region was easy to distinguish because there were no particles in the bleed flow. Figure 8 shows how this entrainment length varies with bleed. Each point represents the average of measurements on five photographs.

The entrainment length shown here is considerably shorter than the vortex formation distance used by Bearman and by Wood. The present photographs

show that for low bleed rates the entrainment process is always completed quite sharply a short distance upstream of the first strong vortices. Gerrard (1966) has explained how the mixing process is in fact completed by the induced cross flow upstream of the most recent strong vortex of the street. This sweeps external fluid across from the opposite side of the wake and reverses some of it into the base region. Such an explanation is quite consistent with the present observations. Many photographs show the unmixed base fluid region to be slightly tapered but with a definite truncated form just upstream of the first vortices.

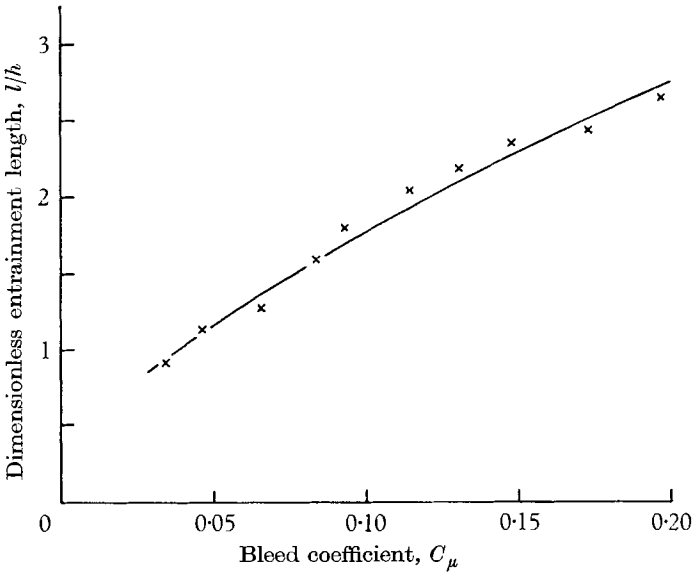

FIGURE 8. Increase of entrainment length with bleed.

The Gerrard model also provides a possible explanation of the increase of entrainment length with bleed. If, as Gerrard suggests, only a limited amount of low velocity wake fluid can be drawn into the vortices as they form, then the increased entrainment required to remove the additional bleed fluid can only take place in the shear layers. Consequently, the length of the shear layers will increase as the bleed flow increases.

As the bleed rate increases still further (figures 6, 7, plate 3) a new type of wake develops, in which the violent mixing associated with strong vortices is apparently no longer needed. The unmixed base fluid region loses its truncated form and becomes almost pointed. Here the entrainment is obviously completed entirely by the shear layers.

It is at these intermediate bleed rates that several observers have noticed that the periodicity of the wake ceases to be regular and becomes intermittent. In 1963, Nash, Quincey & Callinan commented upon the occurrence of intermittent vortex shedding in transonic flow, while some strobotorch observations reported by the present author (Wood 1964) could also be interpreted in this way. This phenomenon is clearly the cause of the poorly defined shedding frequency, which is found as the bleed rate increases.

The present visual study helps to clarify this particular detail. The photographs show that at medium bleed rates the regular vortex pattern is sometimes present and sometimes absent, particularly near the body (figures 3, 4). After watching the development of the wake as a whole during a large number of runs, it became clear that this intermittency was due to a low-frequency cyclic process with a period from ten to thirty times that of normal shedding.

In this cycle, the long irregular turbulent wake was first disturbed by the shedding of three or four symmetrical pairs of vortices. One such pair is visible in figure 6. However, the symmetrical mode was obviously unstable, since the vortices shifted rapidly into the familiar antisymmetrical mode. Once this mode was established, several more strong vortices were shed in the same pattern. Even this process was shortlived, however, and as the vortices passed downstream, the wake degenerated again into the initial irregular form. This fluctuating type of flow marked the onset of an instability, which at higher bleed rates distorted the vortex street into a confused and tortuous collection of vortex tubes. Ultimately these could not be distinguished from the rest of the wake turbulence.

5. Estimation of base pressure

It is commonly recognized that the pressure coefficient is uniform across the thickness of the base region and that in steady flow it is related to the local velocity U_b just outside the separating boundary layers. The usual equation, derived from Bernouilli's equation is

$$-C_{pb} = (U_b/U)^2 - 1,$$

where U is the velocity in the undisturbed stream.

On the present photographs, the streak lengths represent velocities relative to the undisturbed stream. If the streamwise and normal velocity components u and v are measured near the base separation points, then the base pressure can be calculated by means of the corresponding equation

$$-C_{pb} = 2u/U + (u/U)^2 + (v/U)^2.$$

To test this method, a separate experiment was carried out. The base cavity of the present model was first blocked so that the pressure observed was that associated with a solid base rather than a cavity (see §5). Five runs were then photographed, all at the same Reynolds number of $1{\cdot}24 \times 10^4$, based on the model chord. On each of these photographs, three or four particle streaks were measured on each side of the base and the corresponding velocity components were used to compute the base pressure. The values of $-C_{pb}$ differed from one photograph to another, varying between 0·46 and 0·58. The average value of 0·51 is marked in figure 9.

To check the result, a solid wooden model was constructed to a reduced scale and was tested in a wind tunnel over a range of Reynolds numbers including the water tank value. The pressures, measured at a single tapping in the centre of the base agreed well with the tank result (figure 9).

The unsteady nature of the flow is, of course, neglected in the equations used above. However, it is clear that no great error is introduced in the present case

It was concluded, therefore, that in the present base bleed experiments, the mean base pressures could be estimated from the photographs by means of Bernouilli's equation, provided that an average was taken over several photographs.

Following this conclusion, a further set of photographs was taken of the flow about the base of the model. The bleed values were the same as in the previous

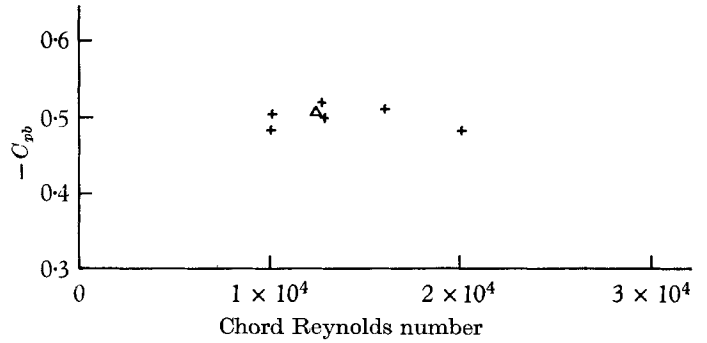

FIGURE 9. Test of pressure estimation method with solid base model. +, manometer readings in air; △, average from five photographs in water.

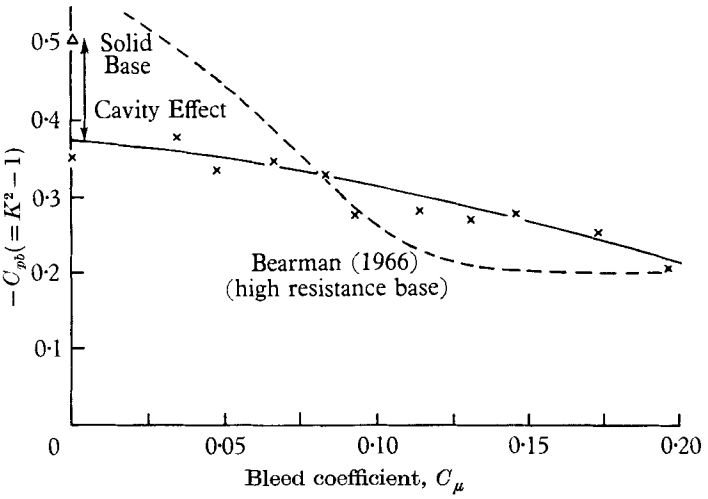

FIGURE 10. Variation of base pressure with bleed.

set so that at least five photographs were available at each bleed rate. Two particle lengths were measured just outside the separating boundary layer on each side of the model. The corresponding pressures were then calculated and averaged to produce the points for figure 10. Here the pressure coefficient rises from an initial value of $-0{\cdot}375$ to $-0{\cdot}21$ at $C_\mu = 0{\cdot}2$. The expected levelling off of the curve does not appear; presumably because the range of bleed rates was not quite large enough. This is surprising because in previous experiments (Wood 1964; Bearman 1966), most of the drag reduction was achieved with bleed coefficients of only 0·1. It may be significant that both the experiments quoted were performed in the presence of relatively thick, turbulent boundary layers, whereas

those in the present case were laminar and might be expected to lead to a more clearly defined vortex street. With this type of flow, it is reasonable to suppose that the periodicity would be more difficult to eliminate. Clearly, this point requires further investigation.

Cavity effect

It is interesting to observe that at zero bleed, the pressure on the hollow base is approximately 25 % higher than on the solid base (figure 10). This cavity effect has been investigated by Nash *et al.* (1963), who observed a 20 % change in pressure. The present experiments were not designed to investigate this effect; nevertheless, one further observation is made possible by the unintentional similarity between the present model and that used by Bearman 1966. The external geometry and flow conditions do not differ sufficiently to account for the large differences between the two curves in figure 10. The only major difference lies in the fact that, in attempting to produce a uniform bleed flow, Bearman covered his base cavity with a high resistance porous material, which was effectively solid. Consequently the major differences between the two results may be interpreted to deduce further information about the cavity effect. It may be concluded from figure 10 that the apparent effectiveness of base bleed on the Bearman model is greatly magnified by the unusual absence of a base cavity. For bleed rates large enough to destroy the vortex street, the base pressures are almost equal, whereas the solid base model has a much lower base pressure at zero bleed. Clearly the beneficial effect of a cavity is associated with the existence of a fluctuating flow, and disappears progressively as the flow becomes steady. This conclusion is entirely consistent with the observations of Nash *et al.* (1963) who noted that when periodicity was eliminated due to supersonic flow, the cavity effect also disappeared.

6. Measurements of vortex spacing and strength

From measurements on individual photographs, the average spacing a of vortices on one side of the street was found to remain approximately constant, over the present bleed range, at three times the base height h (figure 13). Constant vortex spacing had previously been deduced from measurements of shedding frequency in air (Wood 1964). In the present case, because the velocities of the vortex centres are low, the reverse argument may be used to infer that the frequency is not greatly affected by bleed.

The lateral spacing was not measured because the relative longitudinal motion between the vortices and the camera, although small, causes an unknown lateral displacement of the apparent vortex centre away from the real centre (Hooker 1936).

To estimate the strengths of individual vortices, a large number of velocity measurements were made on circles, which enclosed the vortex centres. For this purpose, the centre of the chosen vortex was placed on the centre of a rotating table under a two component travelling microscope. One component was used to move the microscope to a predetermined radius and the turntable was rotated to

find a particle streak. The tangential component of the streak length was then measured on the second microscope axis. By plotting the tangential velocity against the angular position of the turntable, a graph was obtained, whose area was proportional to the circulation.

Preliminary measurements of a few vortices were made at radii of 1·0 and 1·5 cm. These showed that where the vortices appeared to be well formed, 90–95 % of the vorticity in the larger circle was also enclosed by the smaller circle.

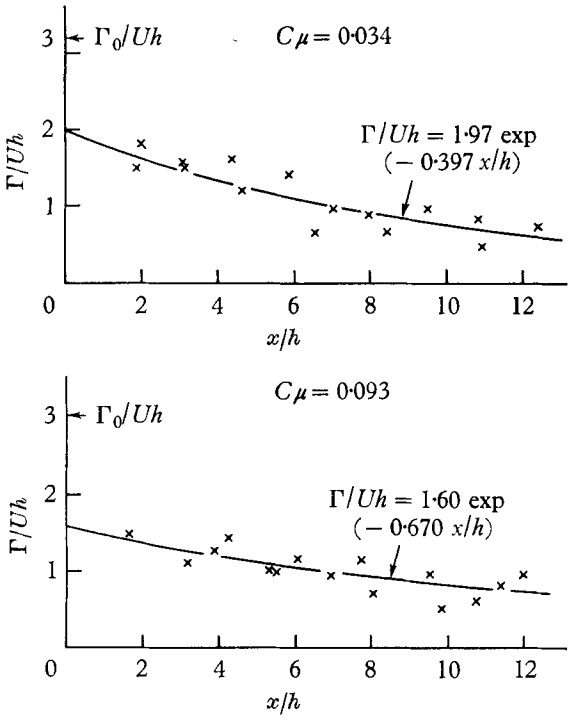

FIGURE 11. Spatial decay of vortex strength (typical curves).

However, this fraction dropped to 80 % in certain other cases. It was not possible to take a still larger radius because adjacent vortices were rarely more than 3 cm apart. Therefore, a radius of 1·5 cm was chosen and the values of Γ shown below represent the circulation on this radius, which was equal to 0·35 times the base height of the model.

Figure 11 shows two typical plots of the dimensionless vortex strength Γ/Uh against position x/h. There is no indication of regular spacing here because the points are taken from several different photographs. The large scatter is also caused largely by differences between individual photographs. It represents time variations in the observed vortex street. This data was plotted for all bleed rates, which produced separate vortices. Surprisingly, the points followed the general trend quite well even for isolated vortices in highly irregular wake patterns.

Despite the scatter, the data shows a consistent spatial decay of vortex strength, which is a result of viscous dissipation. To produce good mean curves, statistical methods were used to compute exponential decay curves with mini-

mum deviation. The majority of these curves showed a decay to half strength between $x/h = 2$ and $x/h = 10$.

To show the effect of bleed, the data from these computed curves was cross-plotted at two streamwise stations (figure 12). Again the large scatter made necessary the use of statistical methods, this time to plot the optimum straight lines.

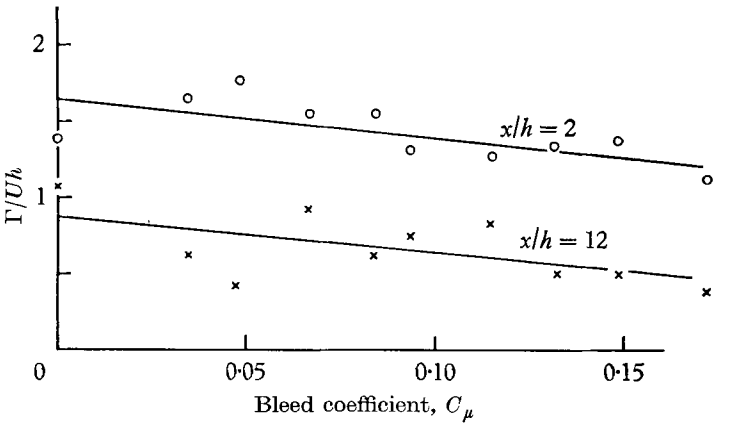

FIGURE 12. Decay of vortex strength with bleed.

These lines show a tendency for the vortex strength to decrease with increasing bleed. They are very nearly parallel, which suggests that the spatial rate of decay is not altered by bleed. Consequently there remain only two factors which contribute to this decrease. One is an increased loss of vorticity from the shear layers before the street is formed. The other is of course a decrease in the actual rate of shedding vorticity from the model, due to changes in base pressure and bleed velocity. The second effect can be evaluated as shown below, and this makes it possible to assess the relative importance of the two effects.

The rate of shedding of vorticity in a shear layer, which is parallel to the flow direction, is given in terms of the average velocities $\overline{U}_b$ and V_j in the external stream and in the wake (figure 1) by the well established expression

$$d\Gamma/dt = (\overline{U}_b^2 - V_j^2)/2.$$

The comparison with the strength Γ of an individual vortex is made easier if this rate of shedding is expressed as the maximum possible strength Γ_0 of a vortex in a von Kármán street, which has the same longitudinal spacing a as the actual street.

Thus we may write

$$(\overline{U}_b^2 - V_j^2)/2 = U\Gamma_0/a - \Gamma_0^2/a^2\sqrt{8}.$$

To introduce the present dimensionless notation we may write

$$\gamma = (\Gamma_0/Uh) \times (h/a), \quad K = \overline{U}_b/U \quad \text{and} \quad C_\mu = V_j/U.$$

The above equation then becomes a quadratic in γ, which has the solution

$$\gamma = \sqrt{2} \pm \{2 - \sqrt{2}(K^2 - C_\mu^2)\}^{\frac{1}{2}}.$$

Here, the negative sign is seen to be appropriate by examining the particular case where the bleed velocity is equal to the external velocity ($K = C_\mu$) and the net vorticity is zero on both sides of the wake.

These equations show that for the present fixed value of a/h (figure 13) the ideal vortex strength Γ_0 decreases, partly because the bleed velocity decreases and partly because the base pressure rises and K falls (figure 10).

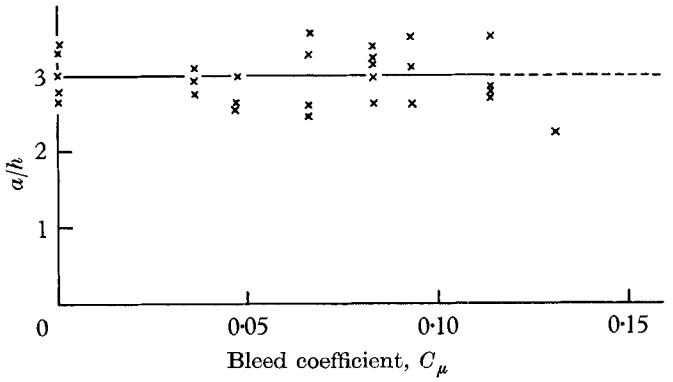

FIGURE 13. Effect of bleed on vortex spacing.

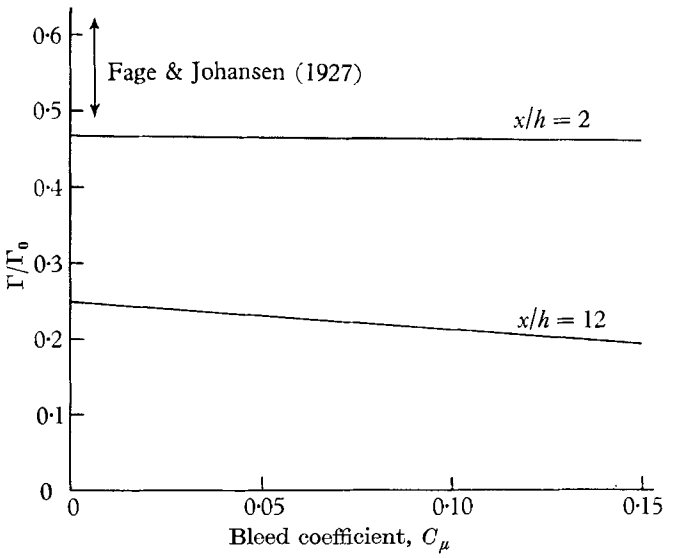

FIGURE 14. Relative vortex strength comparison.

The ratio Γ/Γ_0 may now be used to compare the flux of vorticity in the stres with that shed from the separation points (figure 14). This ratio still decrease with increasing bleed, but at a reduced rate. A comparison between figures 12 and 14 shows, for example, that a 40 % decrease in vortex strength at $x/h = 12$ is reduced to only 25 % when expressed as a ratio with Γ_0. A similar conclusion results from a comparison at $x/h = 2$. Thus the decrease in the shedding rate accounts for nearly half the vortex strength reduction, while the remainder must be due to an increase in the vorticity loss in the shear layers before the vortices are formed. Even at zero bleed, more than half the shed vorticity is lost in this

way. Fage & Johansen found a result similar to this in 1927, while Gerrard (1966) has discussed the mechanism of the loss in detail and has shown that it could be a fundamental part of the vortex formation process.

It must be remembered that the present results are based on a statistical analysis of some very scattered points and the results cannot be regarded as accurate. However, with some caution, the conclusion may be drawn that in the present case the reduction in the rate of shedding, and the subsequent increase in the loss of vorticity are probably similar in magnitude. Consequently both effects must be included in any explanation of the bleed mechanism.

7. Conclusion

The present investigation confirms that small base bleed flows displace the formation region of the vortex street away from the body, although the spacing and frequency are virtually unchanged. At a given streamwise position, the average strength of the vortices is reduced. As far as can be judged from the present scattered results, this is partly due to a reduction in the rate at which vorticity is shed from the model, and partly due to an increase in the vorticity lost in the mixing region. An entirely separate effect is the viscous decay of the vortices once they are formed. This reduces the strength of the street by half within the first ten base heights, and it is not affected by bleed.

The initial displacement of the vortex street is associated with an extension of the unmixed base flow region of the wake. On the basis of the flow model of Gerrard (1966) it may be suggested that the associated increase in the length of the shear layers is necessary in order to entrain the additional bleed fluid. Under these conditions, the entrainment is certainly assisted by the formation of the vortices, which cause a distinct truncation of the unmixed region. However it is clear that this effect must decrease as the vortices become weaker, so it is the shear layers which must provide the extra mixing. If this interpretation is correct, then the need to extract low velocity fluid from the low pressure base region is clearly an important factor in determining the nature of the flow. At higher bleed rates, the higher streamwise momentum imparted by the bleed flow and the higher local pressure both combine to assist the escape of the base fluid. Thus it is hardly surprising that when C_μ exceeds 0·15, the present photographs show the completion of the mixing process by the shear layers alone without the aid of the vortex street. Under these conditions the regular shedding of vortices ceases, intermittently at first, and then completely. The logical conclusion to this line of reasoning, therefore, is to inquire whether it is possible that a vortex street forms in the wake of a bluff body only when the shedding of vortices is necessary to maintain the required rate of entrainment in the dead fluid region near the base. The author is of the opinion that further investigation of this entrainment mechanism would be profitable.

The author wishes to acknowledge the financial assistance of the Science Research Council, which has supported this project with a research grant no. B/SR/822.

REFERENCES

BEARMAN, P. W. 1965 Investigation of the flow behind a two-dimensional model with a blunt trailing edge and fitted with splitter plates. *J. Fluid Mech.* **21**, 241.

BEARMAN, P. W. 1966 Investigation into the effect of base bleed on the flow behind a two-dimensional model with a blunt trailing edge. *AGARD Conf. Proc.* **4**, 497.

CLUTTER, D. W., SMITH, A. M. O. & BRAZIER, J. G. 1962 Techniques of flow visualization using water as the working medium. *Douglas (El Segundo) Rept.* no. Es 29075.

FAGE, A. & JOHANSEN, F. C. 1927 On the flow of air behind an inclined flat plate of infinite span. *ARC R & M* no. 1104.

GERRARD, J. H. 1966 The mechanics of the formation region of vortices behind bluff bodies. *J. Fluid Mech.* **25**, 401.

HOERNER, S. F. 1958 Fluid Dynamic Drag 3-12. (Published by the author).

HOOKER, S. G. 1936 The spacing ratio of a vortex street. *Proc. Roy. Soc.* A 154, 67.

HORLOCK, J. H. 1956 An investigation of the flow in manifolds with open and closed ends. *J. Roy. Aero. Soc.* **60**, 551.

NASH, J. F. 1962 A review of research on two-dimensional base flow. *Nat. Phys. Lab. Aero. Rept.* 1006.

NASH, J. P., QUINCEY, V. E. & CALLINAN, J. 1963 Experiments on two dimensional base flow at subsonic and transonic speeds. *Nat. Phys. Lab. Aero. Rept.* 1070.

WOOD, C. J. 1964 The effect of base bleed on a periodic wake. *J. Roy. Aero. Soc.* **68**, 643.

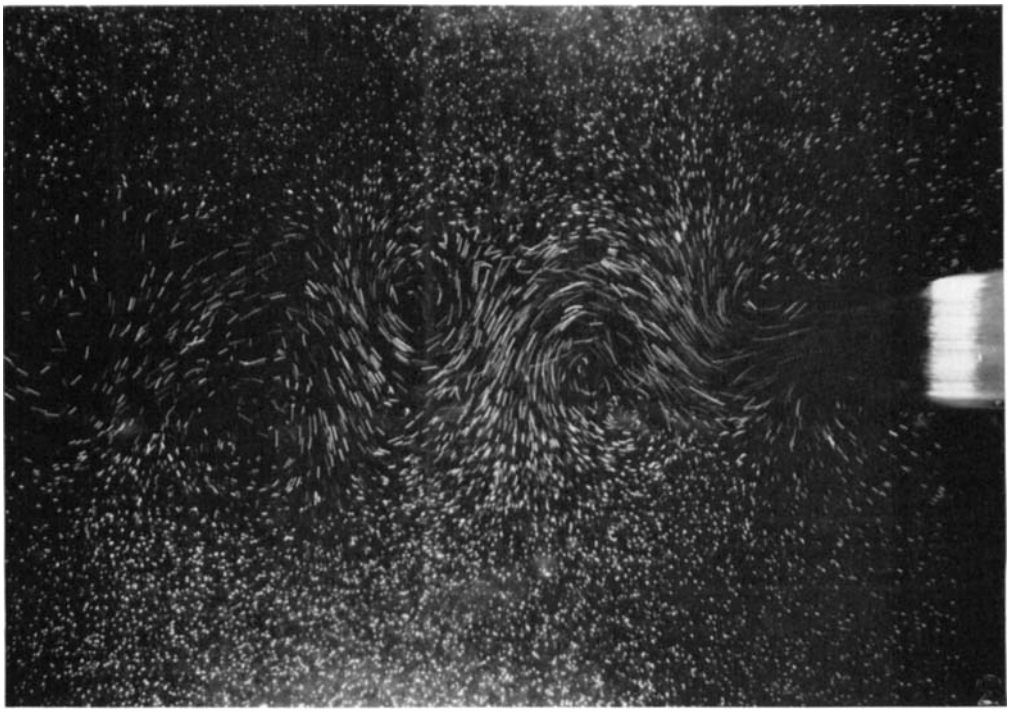

FIGURE 2. $C_\mu = 0$.

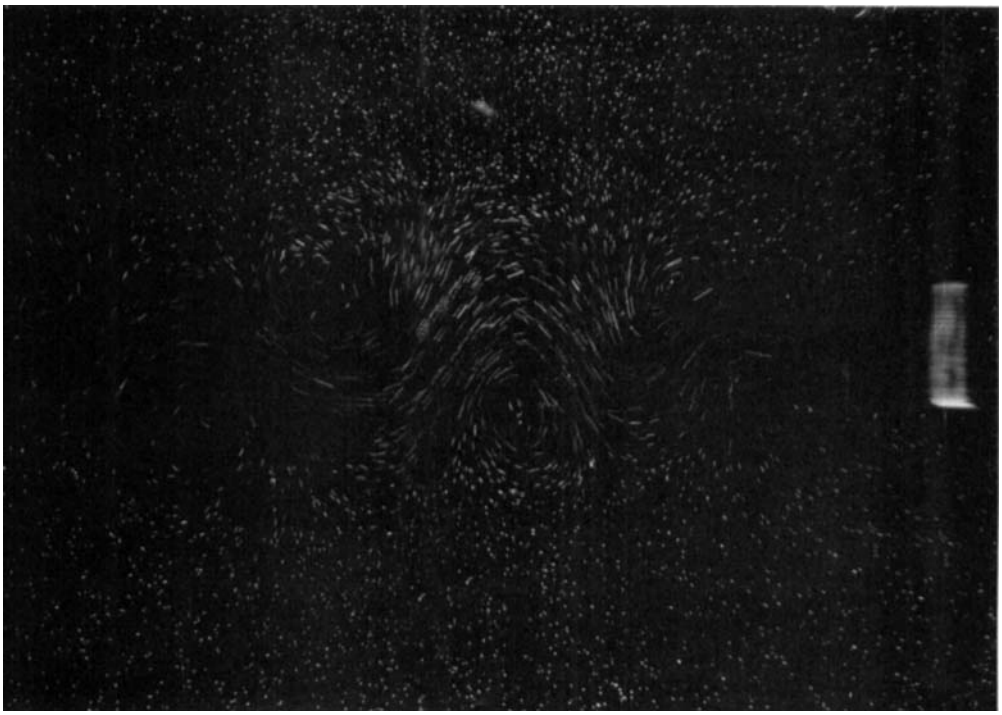

FIGURE 3. $C_\mu = 0{\cdot}083$ (regular wake).

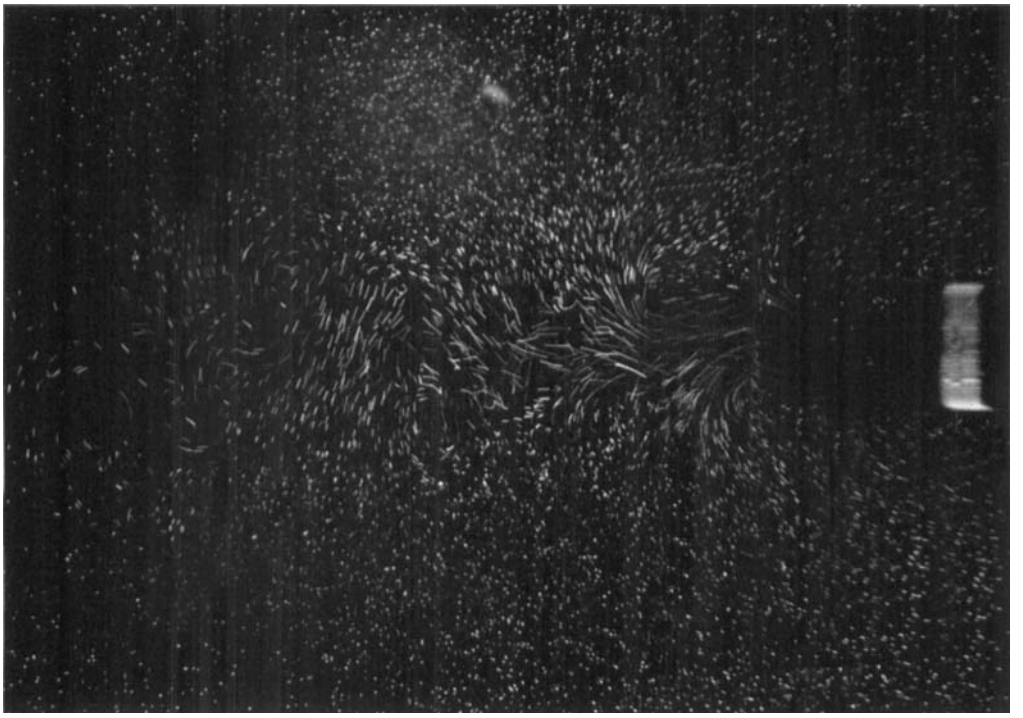

FIGURE 4. $C_\mu = 0{\cdot}083$ (irregular wake).

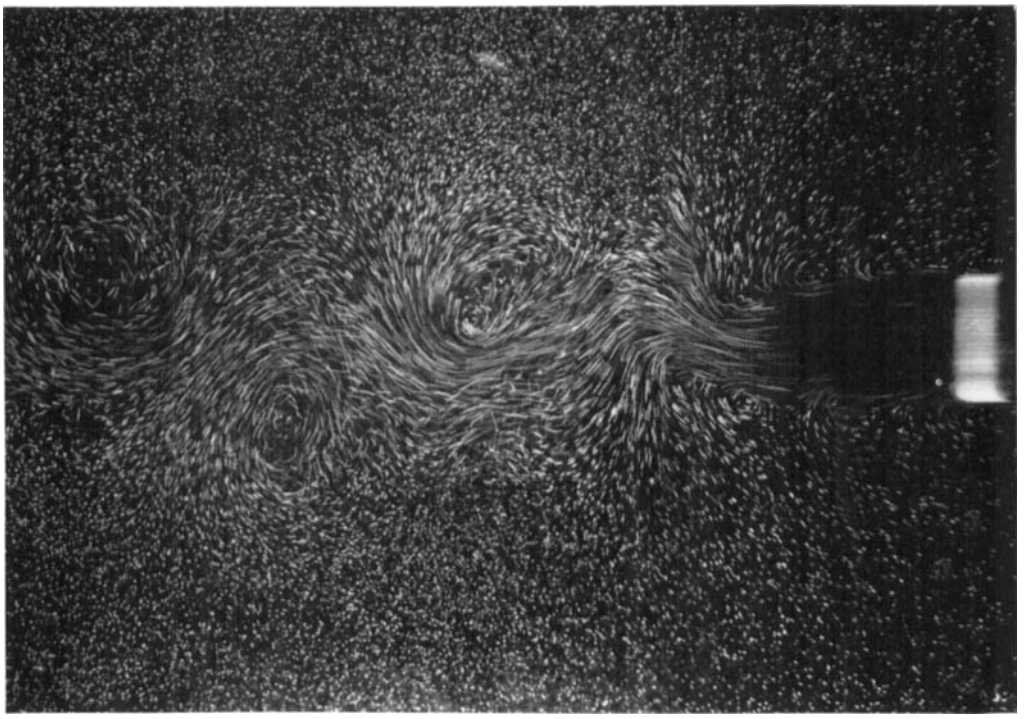

FIGURE 5. $C_\mu = 0{\cdot}093$.

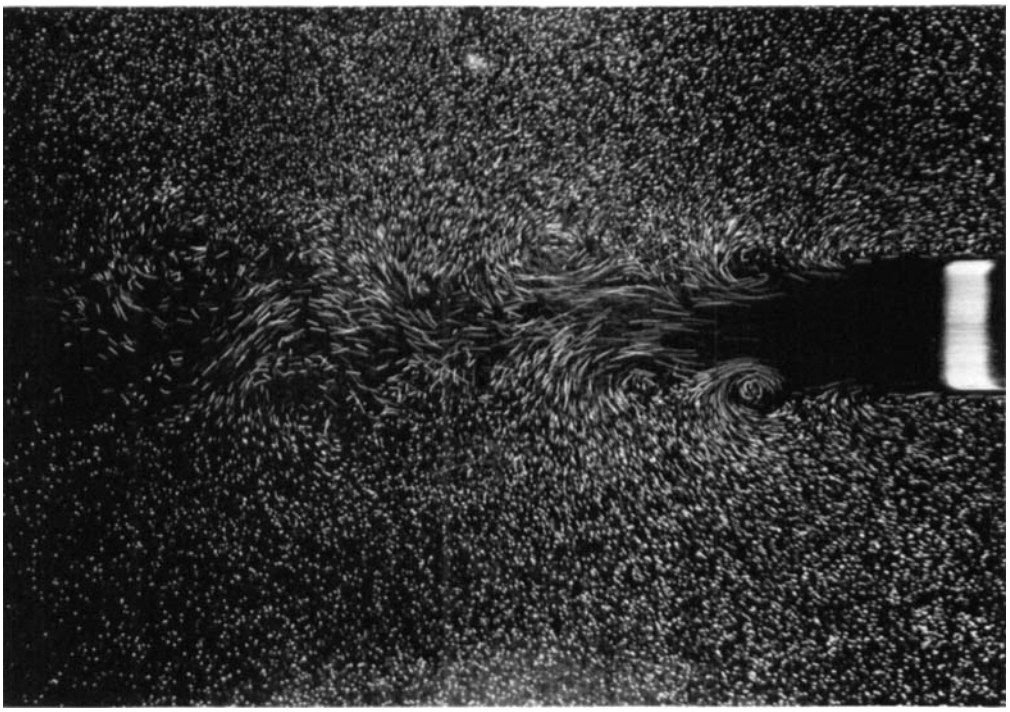

FIGURE 6. $C_\mu = 0{\cdot}146$.

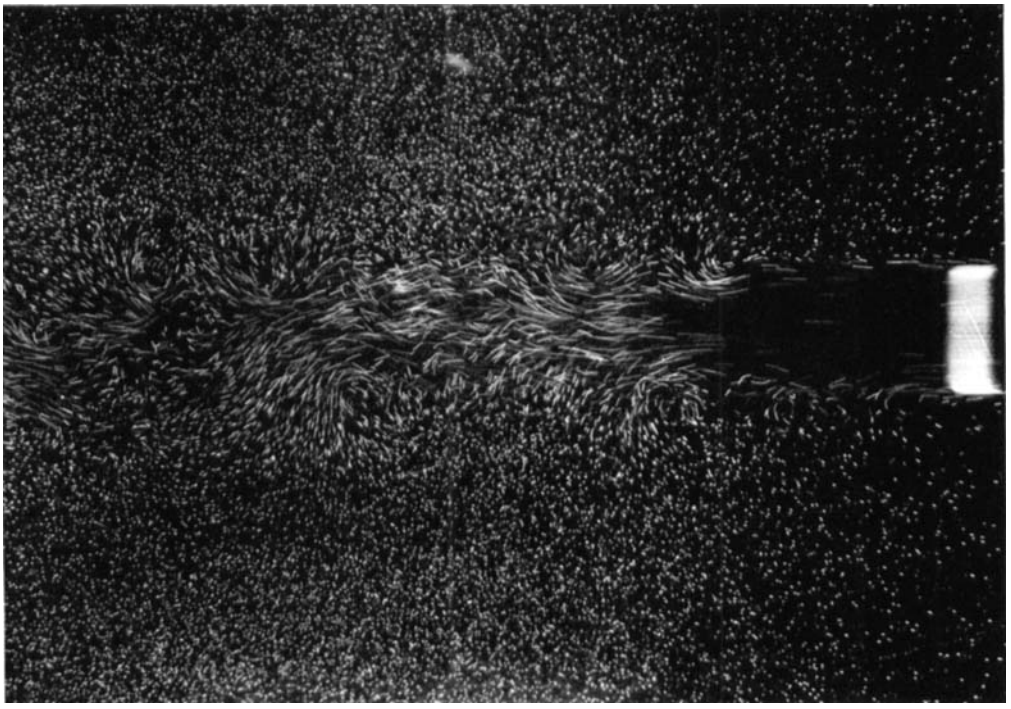

FIGURE 7. $C_\mu = 0{\cdot}196$.